20. Cheluzska P. Computer-aided design of robotised technology for manufacturing working units of mining machines. *International Journal of Mining, Reclamation and Environment*. 2015. Vol. 29, Iss. 1. pp. 62–81.
21. Cheluszka P., Mikuła S., Mikuła J. Conical picks of mining machines with increased utility properties — Selected construction and technological aspects. *Acta Montanistica Slovaca*. 2021. Vol. 26(2). pp. 195–204.
22. Talerov M. P., Bolobov V. I. Life and failures of tangential-rotary picks. *Gornyi Zhurnal*. 2018. No. 4. pp. 77–81.
23. Sementsov V. V., Prokopenko S. A., Ludzish V. S., Abramov V. V. Design and industrial testing of innovative nonexpendable picks for cutter-loaders. *Eurasian Mining*. 2019. No. 2. pp. 59–63
24. Jeong H., Jeon S. Characteristic of size distribution of rock chip produced by rock cutting with a pick cutter. *Geomechanics and Engineering*. 2018. Vol. 15, Iss. 3. pp. 811–822.
25. Bołoz Ł., Kalukiewicz A., Galecki G., Romanyshyn L., Romanyshyn T. et al. Conical pick production process. *New Trends in Production Engineering : Conference*. 2020. Vol. 3, Iss. 1. pp. 231–240.
26. Krauze K., Mucha K., Wydro T., Pieczora E. Functional and operational requirements to be fulfilled by conical picks regarding their wear rate and investment costs. *Energies*. 2021. Vol. 14, Iss. 12. 3696.
27. Zhabin A. B., Polyakov A. V., Averin E. A., Linnik Yu. N., Linnik V. Yu. Ways of development for the theory of rock and coal destruction by picks. *Ugol*. 2019. No. 9. pp. 24–28.
28. Shemyakin S. A., Shishkin E. A. Physical and mathematical model of rock destruction by a milling machine cutter. *Journal of Mining Institute*. 2021. Vol. 251. pp. 639–647.
29. Schopenhauer A. Uber das Interessante. Arthur Schopenhauers sämtliche Werke… München : R. Piper & Co., 1924.
30. What is natural stone cut with. Selection of a technology. Good stone. Available at: https://goodstones.ru/chem-rezhut-prirodnyj-kamen-vybor-texnologii/ (accessed: 30.01.2024).
31. Conical elements. Mining industry. Kennametal. Available at: https://www.kennametal.com/ru/ru/products/mining/underground-mining/conicals.html (accessed: 17.11.2023).
32. Cutting picks for BETEK heading and shearing machines. Available at: http://spsprom.ru/rezczy-dlya-prohodcheskih-i-dobychnyh-kombajnov (accessed: 17.11.2023).
33. Losev V. F., Morozova E. Yu., Tsipilev V. P. Physical basics of laser treatment of materials : Tutorial. Tomsk : TPU, 2011. 199 p.
34. Khoreshok A. A., Mametyev L. E., Tsehin A. M. et al. Mining machines and machine systems. Cutting tool of mining machines : Tutorial. Kemerovo : KuzGTU, 2018. 288 p.
35. Horoshavin L. B. Dialectical development of engineering sciences and convergent technologies. Part 2. Available at: http://www.refractories1.narod.ru (accessed: 30.01.2024).
36. Kashirin V. P. General theory of technology and engineering sciences. *Nauka i technologiya*. 1992. pp. 108–133.
37. Kharin Yu. A. Philosophy : University textbook (8th edition). Minsk : TeatraSistems, 2006. 448 p.
38. Kaplan L. A. New approach to the analysis and resolution of contradictions : Dissertation for certification of Master of TRIZ (theory of inventive problem solving). Hwaseong, South Korea, 2011. 188 p.
39. Prokopenko S. A., Ludzish V. S., Kurzina I. A. Improvement of cutting tools to increase the efficiency of destruction of rocks tunnel harvesters. *Journal of Mining Science*. 2016. Vol. 52, No. 1. pp. 153–159.
40. Prokopenko S. A., Botvenko D. V., Ravochkin N. N., Shadrin V. G. Worn cutter picks as a secondary resource for manufacturing modular cutting tools for shearers. *Eurasian Mining*. 2022. No. 2. pp. 67–70.
41. Dictionary of philosophy. Ed. by Frolova I. T. 7th edition, revised and amended. Moscow : Respublika, 2001. 719 p.
42. Prokopenko S. A., Ludzish V. S., Li A. A. Recycling possibilities for reducing waste from cutters on combined cutter-loaders and road builders. *Waste Management and Research*. 2017. Vol. 35, Iss. 12. pp. 1278–1284. EM

UDC 622.24

***Zh. B. TOSHOV*[1]**, *Dean, Professor, Doctor of Engineering Sciences*
***M. G. RAHUTIN*[2]**, *Professor, Doctor of Engineering Sciences, rahutin.mg@misis.ru*
***B. R. TOSHOV*[3]**, *Associate Professor*
***B. N. BARATOV*[4]**, *Dean, Candidate of Engineering Sciences*

[1] Tashkent State Technical University named after Islam Karimov, Tashkent, Uzbekistan
[2] NUST MISIS, Moscow, Russia
[3] Navoi State Mining and Technology University, Navoi, Uzbekistan
[4] NUST MISIS' Division in Almalyk, Almalyk, Uzbekistan

TRACKING PREVENTION IN ROLLER CONE BIT DRILLING

In the world practice of open pit mining, drilling is mainly carried out using roller cone bits. The cost of drilling totals 25–40% of the overall cost of mining. One of the factors which worsen drilling efficiency is tracking which occurs when spiked teeth of the cones fall into the same craters cut during previous rotations of the bits, and which increases wear of the drilling tool and decreases the rate of drilling.

This article proposes a calculation algorithm for the contact paths of teeth in the peripheral rows of roller cones using actual involutes of toroidal surfaces in the periphery of the well bottom. The algorithm provides a sufficiently accurate mesh of coverage of the well bottom periphery by tricone drill bits with the offset spin axes of roller cones with a view to preventing tracking.

The proposed algorithm can be used for the design and reasonable selection of the roller cone bits with regard to geological conditions of drilling.

Keywords: *roller cone bit, tracking, peripheral teeth row, path, contact points, coverage mesh, tooth*

DOI: *10.17580/em.2024.01.15*

Introduction

At the most open pit mines in the world, drilling operations mainly use roller cone bits, except for drilling in very strong and hard rocks which are drilled with diamond drill bits [1, 2].

Reduction of drilling cost is achievable through the optimized choice of the drilling mode and drilling tool [3]. Optimization of geometrical parameters, headway cost saving and increase in durability of drill bits are the source of enhanced efficiency of the drilling tools [4, 5].

One of the most common phenomena which decrease efficiency of well bottom drilling is tracking [6, 7].

Tracking occurs when destructive elements — tungsten–carbide or steel teeth — fall into the craters cut during previous rotations of a drill bit. Drilling efficiency drops as a result as the well bottom breaks at the contact with tooth surfaces rather than with the space between them. This leads to the increased wear of the drill bit because of the one-sided wear of its teeth, and to the drop in the rate of penetration [8, 9].

The main anti-tracking approaches are the increase in the axial force applied to the drill bit and the decrease in the space between the cutting elements in combination with the increase in their number [10]. The increase in the axial force decreases endurance of a drill bit which is a nonrecoverable object. The increase in the number of cutting elements increases the drill bit cost, the energy input and the probability of the drill teeth chippage [11, 12].

Thus, the contact path computation for the tips of teeth in the peripheral rows of tricone drill bits using involutes of actual toroidal surfaces in well bottom zones can enable proper arrangement of the teeth without changing their number, and is a promising anti-tracking method [13].

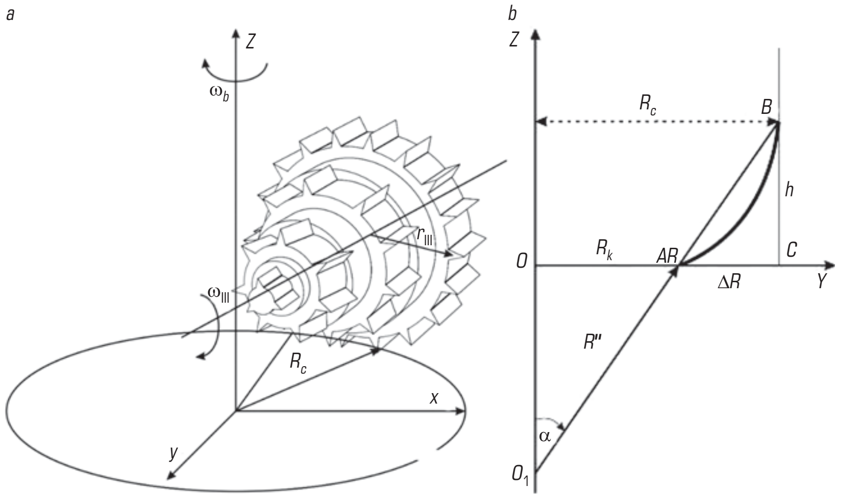

Fig. 1. Diagrams of rolling (*a*) and construction of involuted toroid loop of roller cone (*b*)

Object and Method of Study

The object of study was a roller cone bit with a diameter of 244.5 mm as schematically shown in **Fig 1*a***. Where ω_b — bit rotation speed, rad/s; ω_{III} — cone rotation speed, rad/s; R_c — radius of the well, mm; r_{III} — radius of the cone, mm.

Tricone bits with offset axes of rolling cones form a toroidal surface in the periphery of well bottom [14–16]. In the plane of the radial section of a well, i.e. in the coordinates *ZOY*, the cross-section of the toroidal surface can be presented as the curve *AB* (Fig. 1):

$$\left.\begin{aligned} x &= R\sin\varphi - r\sin\psi\cos\varphi - r\left(1-\cos\psi\right)\sin\varphi\cos\alpha, \\ y &= R\cos\varphi + r\sin\psi\sin\varphi - r\left(1-\cos\psi\right)\cos\varphi\cos\alpha, \\ z &= r\left(1-\cos\psi\right)\sin\alpha; \end{aligned}\right\}, \qquad (1)$$

where R is the radius of a circle along which a teeth row rolls, mm; r is the radius of the rolling row, mm; α is the angle between the row plane and the plane of the well cross-section, deg; ϕ is a variable parameter of the drill bit, deg.

Apparently, the curve *AB* has a varied radius of curvature, and it is required to find the other ways of meshing the coverage areas of toroidal surfaces in the well bottom periphery as opposed to meshing the coverage zones of spherical surfaces in operation of single roller cone bits [17].

Results

The procedure of constructing an involute curve of a toroidal loop is similar to the procedure for the involutes of spherical rings [17, 18]. It is important to know exact values of the upper limit and, in the first place, the lower limit of involutes. Heights of involutes increase one way or another during drawing of actual paths of roller cone teeth in contact with the toroidal surface, and approach the length of the curve *AB*.

Since we know the height h, and the coordinate of the point C, i.e. $OC = R_{max} = R_c$, it is easy to construct an involute of the toroidal loop (see Fig. 1) with regard to the fact that $OA = R_k$, and the radius of the lower limit of the involute is found from the formula:

$$R'' = \frac{R_k}{\cos\left(\operatorname{arctg}\dfrac{h}{\Delta R}\right)}, \qquad (2)$$

where $\Delta R = (R_{max} = R_c) - R_k > R_k$ is the radius of the well bottom circle along which the cone nose row rolls, mm; R_c is the well radius, mm.

The upper limit radius (O_1, B) of the involute is given by:

$$O_1B = \frac{R_c}{\cos\left(\operatorname{arctg}\dfrac{h}{\Delta R}\right)}. \qquad (3)$$

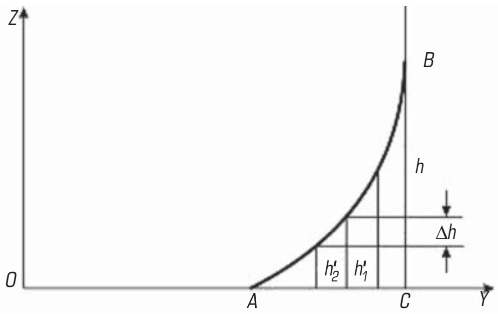

Fig. 2. Diagram of distances from lower limits of toroidal surface to points of curve AB, i.e. heights *h'*, at small increment

With the involute of the toroidal surface in the periphery of well bottom, let us discuss the algorithm of constructing contact paths of teeth edges under the above-specified conditions, i.e. with the parametric equations of the paths of these points in the Cartesian coordinates (1) and at the sufficiently accurate roller cone gear ratios related by the condition $\dfrac{R_0}{r_0} = i = \dfrac{\psi}{\varphi}$ [19, 20].

The calculation algorithm represents the successive evaluation of the following parameters:

1. The distance h'_j from the lower limit of the toroid to a point of the curve.

The set of values of h'_j (**Fig. 2**) is found from partition of the total height $h = BC$ of the toroidal surface, which is a peripheral surface of the well bottom, i.e. the height of the curve *AB*, with a small increment Δh.

2. The path ψ'_j of the teeth row.

The set of values of ψ'_j (**Fig. 3**) is found from calculations using the third equation from (1)

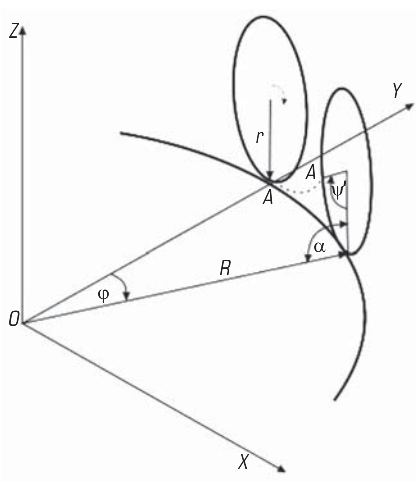

Fig. 3. Parameter ψ'_j

$$z_j = r_j\left(1-\cos\psi\right)\sin\alpha, \tag{4}$$

and initial data from column 1 in Table 1, i.e. from the formula:

$$\psi'_j = \arccos\left(1-\frac{h'_j}{r_j\cdot\sin\alpha}\right). \tag{5}$$

The data set of ψ'_j is important as it leads directly to the system of parametric equations of the trajectory paths in the form of (1). The parameter is not a function of the gear ratio of the roller cone. In other words, the mode of rolling of the peripheral row is of no importance (without frictional sliding, with positive or negative sliding), and the set of ψ'_j is determinable unambiguously by placing h_j in (4) instead of z_j

$$h'_j = r_j\left(1-\cos\psi'\right)\sin\alpha\,. \tag{6}$$

Herefrom we obtain the final formula:

$$\psi'_j = \arccos\left(1-\frac{h'_j}{r_j\cdot\sin\alpha}\right). \tag{7}$$

Naturally, the range of the set of this parameter is limited by the value of h, i.e.:

$$h'_j = 0 \le \psi'_j \le h'_j = h\,.$$

3. The coordinates x_j and y_j of a tooth edge point in projection onto a conditional plane XOY chosen to represent the well bottom.

The data sets of the coordinates of the tooth edge path in projection onto the plane XOY (**Fig. 4**), x_j and y_j, are generated by calculation from the first two equations in system (1) at the certain rotation of the cone nose row by the angle ψ'_j, i.e. from the formulas:

$$\begin{aligned} x'_j &= R_j\sin\varphi_j - r_j\sin\psi'_j\cos\left(\varphi_j-\gamma_j\right) - r_j\left(1-\cos\psi'_j\right)\sin\left(\varphi_j-\gamma_j\right)\cos\alpha \\ y &= R_j\cos\varphi_j - r_j\sin\psi'_j\sin\left(\varphi_j-\gamma_j\right) - r_j\left(1-\cos\psi'_j\right)\cos\left(\varphi_j-\gamma_j\right)\cos\alpha \end{aligned} \tag{8}$$

when $\varphi_j = \dfrac{\psi'_j}{i}$ and $\gamma = \arcsin\left(\dfrac{k}{R_j}\right)$, where R_j, r_j, α and k are the geometrical parameters of the cone nose row (see Fig. 4).

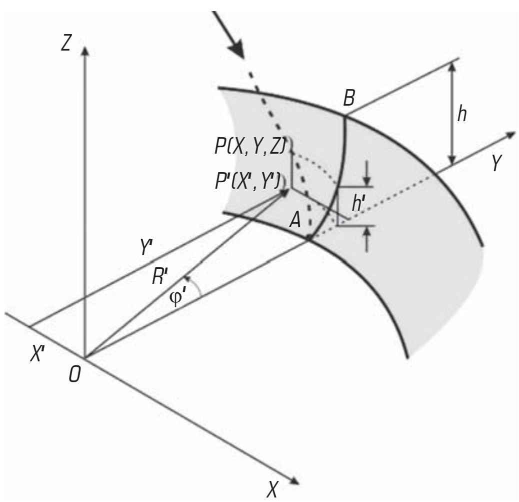

Fig. 4. Diagram of coordinates *X'* and *Y'* of tooth tip motion along toroidal surface at well bottom

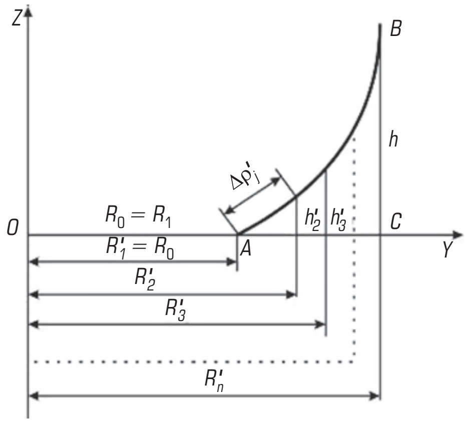

Fig. 5. Pattern of calculation of $\Delta\rho'_j$

The coordinates x'_j and y'_j are the coordinates of motion of the tooth tip in the peripheral row in a new coordinate system $X'_jOY'_j$ which occurs in the same plane as XOY and has the same origin.

4. The rotational angle φ'_j of a tooth edge point in projection onto a plane XOY chosen to represent the well bottom.

The set of data on the parameter φ'_j gives the angles of rotation of the tooth edge point in projection onto the plane XOY. This is not the angle of rotation of the teeth row center round the bit axis, which is given together with the tooth edge point rotation angle φ'_j in Fig. 4.

This parameter is calculated using the ratio

$$\frac{x'_j}{y'_j} = \mathrm{tg}\,\varphi'_j\,, \tag{9}$$

i.e. from the formula:

$$\varphi'_j = \mathrm{arctg}\frac{x'_j}{y'_j}\,. \tag{10}$$

The data set of φ'_j, alongside with the next following data set in the algorithm, is a basis to jump to the polar coordinate system. Evidently, it is impossible to transfer the curves from a toroidal surface to a plane involute at an identical accuracy.

5. The parameter R'_j which is the distance from the drill bit axis to the plane XOY.

The set of the values of R'_j is the distances from the bit axis to a projection of a test point onto the plane XOY (see Fig. 4). This parameter is given by:

$$R'_j = \sqrt{x'^2_j + y'^2_j}\,. \tag{11}$$

Here, we use the Pythagoras theorem at the sufficiently accurately calculated coordinates x'_j and y'_j. The data set of R'_j helps make analogies in the Cartesian and polar coordinates. This point will be explained below.

6. The parameter $\Delta\rho'_j$ which is the distance between peaks.

The set of $\Delta\rho'_j$ is the sum of distances between the neighbor heights h'_j and represents a hypotenuse of rectangular triangles (**Fig. 5**). Generation of this data set is given analytically by:

$$\begin{aligned} &\Delta\rho'_1 = 0, \\ &\Delta\rho'_2 = \sqrt{\left(R'_2-R'_1\right)^2+\left(h'_2-h'_1\right)^2}, \\ &\Delta\rho'_3 = \Delta\rho'_2 + \sqrt{\left(R'_3-R'_2\right)^2+\left(h'_3-h'_2\right)^2}, \\ &-\,- \\ &\Delta\rho'_n = \Delta\rho'_2 + \ldots + \Delta\rho'_{n-1}\sqrt{\left(R'_n-R'_{n-1}\right)^2+\left(h'_n-h'_{n-1}\right)^2}. \end{aligned} \tag{12}$$

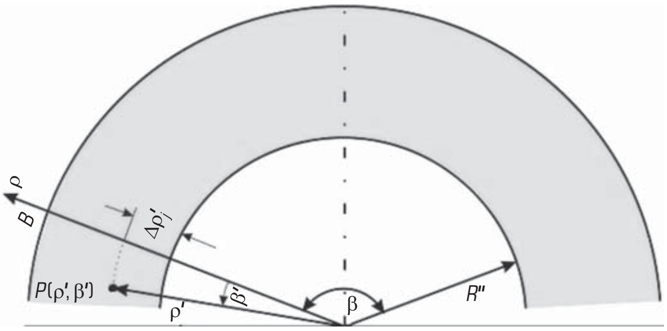

Fig. 6. Presentation of parameters ρ'_j

Starting from this stage, the algorithm generates directly the analytical structure of the polar coordinates, namely, the radius-vector; the physical sense of the latter will be explained in the next stage.

It should be emphasized that it is unadvisable to increase the values of $\Delta\rho'_j$ without special research. The values of h'_j and R'_j for generating the required data set are taken from columns 1 and 3 in **Table 1**. The value of Δh_j in column 1 of Table 1 should be assumed to equal 1 mm for making the algorithm simpler and more accurate.

7. The parameter ρ'_j which is the radius-vector in the polar coordinates.

The data set of ρ'_j is the radius-vectors in the polar coordinates with the origin at the root of the involute (**Fig. 6**) and is generated by calculations from the formula:

$$\rho'_j = R + \Delta\rho'_j \,. \tag{13}$$

The parameter R'' is determined when constructing the involute of the toroidal surface (see Fig. 6).

Apparently, generation of the data set of the radius-vector ρ'_j is perfectly accurate in constructing involutes of cones.

In this case, we sort of strengthen a concave toroidal surface and mesh the surface using craters made by tips of teeth, making it similar to a real surface.

8. The polar rotation angles β'_j.

The set of values of β' is the polar angles (see Fig. 6), i.e. the angles of rotation of a certain point in the polar coordinates round the origin at the root of the involute. This parameter is calculated based on the equality of the lengths of arcs in the toroidal loop in the Cartesian coordinates and in the involute of the parameter in the polar coordinates, i.e. from the condition:

$$\varphi'_j R'_j = \beta'_j \left(R'' + \Delta\rho'_j\right). \tag{14}$$

Consequently,

$$\beta'_j = \frac{\varphi'_j R'_j}{R'' + \Delta\rho'_j}\,. \tag{15}$$

Now, from the condition of the equality of arcs in the rectangular and polar coordinate systems, the purpose of finding the parameters φ'_j and R'_j, as well as R'' and $\Delta\rho'_j$ becomes evident. Obviously, there is no other way of constructing the paths of the teeth tips in the peripheral rows of roller cone bits in the involutes of the toroidal peripheral surfaces at the well bottom. Generation of the data set of β'_j is carried out at the minimum possible increments of the initial parameters, which are now the arguments of the function represented by the polar angle.

As a case-study, let us consider a tricone drill bit for hole drilling with the diameter of 244.5 mm with the parameters obtained using the proposed algorithm and compiled in **Tables 1**, **2** and **3**.

Roller cone No. 1:
Gear ratio — 1.411;
Peripheral teeth row height — 9.843 mm;
Cone nose radius — 68.000 mm;
Radius of circle along which cone nose row rolls — 121.131 mm;
Cone bottom radius (R'') = = 1072.052 mm;
Angle of involute at lower limit (β'_j) = 40.676 deg.
Roller cone No. 2:
Gear ratio — 1.485;

Table 1. Parameters of roller cone No. 1

h'_j, mm	ψ'_j, deg	x'_j, mm	y'_j, mm	φ'_j, deg	R'_j, mm	$\Delta\rho'_j$, mm	ρ'_j, mm	β'_j, deg
0.00	0.00	0.00	121.13	0.00	121.13	0.000	1072.052	0.000
0.98	–10.66	28.39	118.22	13.50	121.58	1.083	1073.135	1.530
1.97	–15.10	39.81	115.08	19.08	121.77	2.084	1074.136	2.163
2.95	–18.52	48.33	111.91	23.36	121.90	3.078	1075.130	2.648
3.94	–21.41	55.31	108.75	26.96	122.00	4.067	1076.119	3.056
4.92	–23.98	61.27	105.60	30.12	122.09	5.055	1077.107	3.414
5.91	–26.31	66.50	102.46	32.98	122.15	6.041	1078.093	3.737
6.89	–28.46	71.15	99.34	35.61	122.19	7.027	1079.079	4.033
7.87	–30.47	75.35	96.24	38.06	122.23	8.012	1080.063	4.307
8.86	–32.36	79.15	93.16	40.35	122.24	8.996	1081.048	4.563
9.84	–34.17	82.62	90.10	42.52	122.25	9.980	1082.032	4.804

Table 2. Parameters of roller cone No. 2

h'_j, mm	ψ'_j, deg	x'_j, mm	y'_j, mm	φ'_j, deg	R'_j, mm	$\Delta\rho'_j$, mm	ρ'_j, mm	β'_j, deg
0.00	0.00	0.00	121.13	0.00	121.13	0.000	1072.052	0.000
0.98	–10.66	27.61	118.41	13.13	121.58	1.083	1073.135	1.487
1.97	–15.10	38.74	115.44	18.55	121.77	2.084	1074.136	2.103
2.95	–18.52	47.05	112.45	22.70	121.90	3.078	1075.130	2.574
3.94	– 21.41	53.87	109.47	26.20	122.00	4.067	1076.119	2.971
4.92	– 23.98	59.71	106.49	29.28	122.09	5.055	1077.107	3.319
5.91	–26.31	64.83	103.52	32.06	122.15	6.041	1078.093	3.632
6.89	– 28.46	69.41	100.57	34.61	122.19	7.027	1079.079	3.919
7.87	– 30.47	73.53	97.63	36.98	122.23	8.012	1080.063	4.185
8.86	– 32.36	77.28	94.72	39.21	122.24	8.996	1081.048	4.434
9.84	– 34.17	80.71	91.82	41.32	122.25	9.980	1082.032	4.668

Table 3. Parameters of roller cone No. 3

h'_j, mm	ψ'_j, deg	x'_j, mm	y'_j, mm	φ'_j, deg	R'_j, mm	$\Delta\rho'_j$, mm	ρ'_j, mm	β'_j, deg
0.00	0.00	0.00	121.13	0.00	121.13	0.000	1072.052	0.000
0.98	–10.66	28.61	118.17	13.61	121.58	1.083	1073.135	1.542
1.97	–15.10	40.11	114.97	19.23	121.77	2.084	1074.136	2.180
2.95	–18.52	48.69	111.75	23.54	121.90	3.078	1075.130	2.669
3.94	–21.41	55.72	108.54	27.17	122.00	4.067	1076.119	3.081
4.92	–23.98	61.72	105.34	30.37	122.09	5.055	1077.107	3.442
5.91	–26.31	66.97	102.15	33.25	122.15	6.041	1078.093	3.767
6.89	–28.46	71.65	98.98	35.90	122.19	7.027	1079.079	4.065
7.87	–30.47	75.86	95.83	38.36	122.23	8.012	1080.063	4.342
8.86	–32.36	79.68	92.71	40.68	122.24	8.996	1081.048	4.600
9.84	–34.17	83.16	89.60	42.86	122.25	9.980	1082.032	4.843

Peripheral teeth row height — 9.843 mm;
Cone nose radius — 68.000 mm;
Radius of circle along which cone nose raw rolls — 121.131 mm;
Cone bottom radius (R'') = 1072.052 mm;
Angle of involute at lower limit (β'_j) = 40.676 deg.

Roller cone No. 3:

Gear ratio — 1.391;
Peripheral teeth row height — 9.843 mm;
Cone nose radius — 68.000 mm;
Radius of circle along which cone nose raw rolls — 121.131 mm;
Cone bottom radius (R'') = 1072.052 mm;
Angle of involute at lower limit (β'_j) = 40.676 deg.

The calculations show that a drill bit with the roller cones of these sizes excludes tracking as the parameters of the contact points of the peripheral row teeth (x'_j, y'_j, φ'_j, β'_j) have no repeated contacts and angles at a conditional well bottom.

Conclusions

1. The coverage meshing of the involutes of the toroidal surface depends on the cutting structure of the peripheral teeth rows, as well as on the sizes and orientation of the edges of the teeth in the peripheral row relative to the planes of the cone nose rows and to the gear ratios of the roller cones.

2. The authors have proposed the calculation algorithm for the contact paths of teeth tips in the peripheral rows of tricone bits on the actual involutes of the toroidal surfaces in the periphery of well bottoms.

3. The proposed algorithm allows sufficiently accurate coverage meshing of the peripheral zones at well bottoms in tricone bit drilling at offset axes of rotation of roller cones toward anti-tracking.

4. The proposed algorithm can be used for the design and justified selection of drill bits with regard to geological conditions of drilling.

References

1. Baratov B. N., Umarov F. Ya., Toshov Zh. B. Tricone drill bit performance evaluation. *Gorniy Zhurnal*. 2021. No. 12. pp. 60–63.
2. Inoue T., Rheem C.-K., Kyo M., Sakaguchi H., Matsuo M. Y. Experimental study on the characteristics of VIV and whirl motion of rotating drill pipe. *ASME 2013 32nd International Conference on Ocean, Offshore and Arctic Engineering*. 2013. Vol. 7. pp. 9–14.
3. Blinkov O. G. Ways to enhance efficiency of roller cone rock bits : Theses of Dissertation of Doctor of Engineering Sciences. Moscow, 2007. 359 p.
4. Menezes P. L., Lovell M. R., Higgs C. F. III. Influence of friction and rake angle on the formation of discontinuous rock fragments during rock cutting. *STLE/ASME 2010 International Joint Tribology Conference*. 2010. pp. 271–273.
5. Blinkov O. G. Determination of effective geometric parameters of carbide drilling roller bits depending on the mechanical properties of the rocks. *Equipment and Technologies for Oil and Gas Complex*. 2022. No. 1(127). pp. 27–31.
6. Toshov Zh. B., Baratov B. N., Toshniyozov L. G., Ochilov S. T. Technology of drilling tool engineering. *Gorniy vestnik Uzbekistana*. 2018. No. 1. pp. 71–74.
7. Naganawa S. Dynamics modeling of roller cone bit axial vibration. *Journal of the Japanese Association for Petroleum Technolo*gy. 2005. Vol. 70, Iss. 4. pp. 333–337.
8. Shilin Chen. Roller-cone bits, systems, drilling methods, and design methods with optimization of tooth orientation. Patent US, No. 6,412,577 B1. Published: 02.07.2002.
9. A. V. Aaron, V. Litvienko. Antitracking earth boring bit with selected varied pitch for overbreak optimization and vibration reduction. Patent US, No. 7,195,086 B2. Published: 27.03.2007.
10. Blinkov O. G. Study of tracking (rack formation) at the wellbottom. *Construction of Oil and Gas Wells on Land And Sea*. 2021. No. 12(348). pp. 24–28.
11. Das M. K., Sarkar S., Choudhary B. S. Experimental and numerical analysis of rotary tricone drill bit and its wear prediction. *Journal of the Brazilian Society of Mechanical Sciences and Engineering*. 2018. Vol. 40, No. 366. DOI: 10.1007/s40430-018-1292-4
12. Tian J., Zhang T., Dai L., Cheng W., Yang L. et al. Dynamic characteristics and test analysis of a new drilling downhole tool with anti-stick–slip features. *Journal of Mechanical Science and Technology*. 2018. Vol. 32. pp. 4941–4949.
13. Toshov J. B., Toshov B. R., Baratov B. N., Haqberdiyev A. L. Designing new generation drill bits with optimal axial eccentricity. *MIAB*. 2022. No. 9. pp. 133–142.
14. Toshniyozov L., Mamatov M. Analysis of drill bit speed in bit–rock interaction with the use of numerical simulation methods. *Ukrainian School of Mining Engineering — 2020. E3S Web of Conferences*. 2020. Vol. 201. ID 01006.
15. Bulatov A. I. Drilling engineer's handbook : In 4 books. Moscow : Nedra, 1995. 272 p.
16. Benavides-Serrano A. F., Peña-Sabogal A. S., León O. M., Sánchez-Acevedo H. G., González-Estrada O. A. Optimization of parameters in material selection of tricone drill bit head design. *Journal of Physics: Conference Series*. 2019. Vol. 1159. ID 012018.
17. Kryukov G. M. Physics of rock fracture in drilling and blasting. Moscow : Gornaya kniga, 2006. Vol. 1. 330 p.
18. Kricak L., Negovanovic M., Mitrovic S., Miljanovic I., Nuric S. et al. Development of a fuzzy model for predicting the penetration rate of tricone rotary blasthole drilling in open pit mines. *The Journal of the Southern Africa Institute of Mining and Metallurgy*. 2015. Vol. 115, No. 11 pp. 1065–1071.
19. Rahimov R. M. Method to assess working efficiency of one-cone drill bits : Theses of Dissertation of Candidate of Engineering Sciences. Tashkent, 2002. 107 p.
20. Ibragimova P. I. Analysis of functions in energy input pattern in dynamic systems at extremum. *Construction of Oil and Gas Wells on Land and Sea*. 2005. No. 11. pp. 19–25. EM